NTNU
Norwegian University of
Science and Technology

A Novel Approach to Flow Model Turbulence Validation Using a Long Range Pulsed Lidar

Andrea Risan

NTNU

Norwegian University
of Science and Technology

Department of Energy
and Process Engineering

MASTER THESIS

for

Student Andrea Risan

Spring 2017

Estimating turbulence parameters from Lidar measurements

Technical developments have made it possible to construct robust, affordable and reliable Doppler laser anemometers. When pointing the laser into the air the light is scattered in all directions by aerosols and that part of the light, which is reflected into the laser receiver, can be analyzed to determine its power spectrum, the Doppler spectrum. Since the aerosols are in motion the light will change frequency corresponding to the average velocity in a volume, which for most practical applications can be considered a finite line segment aligned the beam direction. The shift in mean frequency, determined by the outgoing and the incoming Doppler spectra, is proportional to the velocity component along the beam direction. Smalikho (1995) discussed this phenomenon in details. There are two modes of laser operation, continuous or pulsed. In the first case the laser is operating continuously and focused at a particular distance. This type of instrument, the CW-laser anemometer, is one subject of the following. We refer to the pioneering work by Smalikho (1995) and Banakh & Smalikho (1997). In the second case, each pulse is analyzed and the distance to the measuring volume is determined by means of pulse time-of-flight. This technique is termed range gating and has the advantage that the velocity can be measured simultaneously at several distances. In both cases the velocity is averaged over a line segment along the laser beam. We call the first type of instrument a CW-laser anemometer (Continous-Wave laser anemometer) and the second a LIDAR anemometer (LIght Detection And Ranging anemometer).

The estimation of turbulence parameters derived from LIDAR measurements is an active and partially controversial field of research that has indicated certain limitations (Lundquist et al (2015), Sathe et al (2011)). Those are mainly related to the inherent general differences between an insitu point measurement by cup or sonic anemometers and a volume-averaged value derived from LIDAR data, as well as from the wind vector reconstruction from subsequent line-of-sight measurements. Frehlich (2012) shows that in the case of the Win-Tracer the measurement error due to volume averaging can be decreased by more flexible velocity estimation statistics that depend on local turbulence conditions. In terms of inaccuracies related to wind vector reconstructions from line-of-sight measurements Towers and Jones (2014) show improvements for two-beam nacelle LIDARs with dynamic wind modeling and state estimation. For four-beam measurements the wind reconstruction is more accurate, but based on the assumption of homogeneous flow during one measurement circle, leading to lower sampling rates. In terms of e.g. wind speed variances, four-beam LIDAR measurements have a limitation in measuring small turbulent length scales compared to e.g. sonic measurements. This limitation is based on the lower LIDAR sampling rate of 1 Hz compared to sonic anemometer measurements taken at

10 -100 Hz. LIDAR measurements can therefore not deliver turbulence information over the complete spectrum of boundary layer turbulence.

The purpose of the present investigation is to establish a basis for remote determining of turbulence fine-structure in terms of specific kinetic energy in the atmospheric boundary layer.

REFERENCES:
Smalikho, I. N. (1995), 'On measurement of the dissipation rate of the turbulent energy with a CW lidar', Atmos. Oceanic Opt. 8 , 788–793.
Banakh, V. A. & Smalikho, I. N. (1997), 'Determination of the turbulent energy dissipation rate from lidar sensing data', Atmos. Oceanic Opt. 10 , 295–302.
 J.K. Lundquist, M.J. Churchfield, S. Lee, A. Clifton, Quantifying error of lidar and sodar Doppler beam swinging measurements of wind turbine wakes using computational fluid dynamics, Atmos. Meas. Tech. 8 (2015) 907e920, http://dx.doi.org/10.5194/amt-8-907-2015.
A. Sathe, J. Mann, J. Gottschall, M.S. Courtney, Can wind lidars measure turbulence? J. Atmos. Ocean. Technol. 28 (7) (2011) 853e868, http://dx.doi.org/10.1175/JTECH-D-10-05004.1.
R. Frehlich, Upstream Measurements of Wind Profiles with Doppler Lidar for Improved Wind Energy Integration, Tech. Rep, Golden Field Office, Golden, CO (United States), oct 2012, http://dx.doi.org/10.2172/1053852.
P. Towers, B. Ll Jones, C.B. Ll Jones, Real-time wind field reconstruction from LiDAR measurements using a dynamic wind model and state estimation, Wind Energy (2014), http://dx.doi.org/10.1002/we.1824.

-- '' --

Within 14 days of receiving the written text on the master thesis, the candidate shall submit a research plan for his project to the department.

When the thesis is evaluated, emphasis is put on processing of the results, and that they are presented in tabular and/or graphic form in a clear manner, and that they are analyzed carefully.

The thesis should be formulated as a research report with summary both in English and Norwegian, conclusion, literature references, table of contents etc. During the preparation of the text, the candidate should make an effort to produce a well-structured and easily readable report. In order to ease the evaluation of the thesis, it is important that the cross-references are correct. In the making of the report, strong emphasis should be placed on both a thorough discussion of the results and an orderly presentation.

The candidate is requested to initiate and keep close contact with his/her academic supervisor(s) throughout the working period. The candidate must follow the rules and regulations of NTNU as well as passive directions given by the Department of Energy and Process Engineering.

Risk assessment of the candidate's work shall be carried out according to the department's procedures. The risk assessment must be documented and included as part of the final report. Events related to the candidate's work adversely affecting the health, safety or security, must be documented and included as part of the final report. If the documentation on risk assessment represents a large number of pages, the full version is to be submitted electronically to the supervisor and an excerpt is included in the report.

Pursuant to "Regulations concerning the supplementary provisions to the technology study program/Master of Science" at NTNU §20, the Department reserves the permission to utilize all the results and data for teaching and research purposes as well as in future publications.

The final report is to be submitted digitally in DAIM. An executive summary of the thesis including title, student's name, supervisor's name, year, department name, and NTNU's logo and name, shall be submitted to the department as a separate pdf file. Based on an agreement with the supervisor, the final report and other material and documents may be given to the supervisor in digital format.

☐ Work to be done in lab (Water power lab, Fluids engineering lab, Thermal engineering lab)
☐ Field work

Department of Energy and Process Engineering, 15. January 2017

Lars Sætran
Academic Supervisor

Research Advisor:

A Novel Approach to Flow Model Turbulence Validation Using a Long Range Pulsed Lidar

Andrea Risan

Department of Energy and Process Engineering

Norwegian University of Science and Technology

June 10, 2017

ABSTRACT

Flow models are useful to predict wind conditions for wind energy production purposes. However, as wind power development expands into areas of even more complex terrain and challenging flow conditions, more research is needed to investigate the ability of such models to describe turbulent flow features. In this study, the performance of a hybrid RANS/LES (DES) model in highly complex terrain has been investigated. The model was compared with measurements from a long range pulsed lidar, which first were validated with sonic anemometer data. The accuracy of the lidar was considered to be sufficient for validation of flow model turbulence estimates. By reducing the range gate length of the lidar a slight additional improvement in accuracy was obtained, but the availability of measurements was reduced due to the decreased intensity of the backscattered signal. The DES model was able to capture the variations of velocity and turbulence intensity along the line-of-sight of the lidar beam but overestimated the turbulence level in regions of complex flow.

Keywords - Detached Eddy Simulation, Turbulence, Lidar, Range Gate Length

I. INTRODUCTION

In recent years, computational fluid dynamics (CFD) have frequently been applied for predicting wind conditions in the wind energy industry. Such flow models can provide a three-dimensional description of the flow field in a large area using input data from point measurements or meso-scale meteorological models. However, although CFD models have become increasingly advanced, the challenge of accurately describing turbulent flow, e.g. in complex terrain, remains. For a large three-dimensional area, the requirement of spatial and temporal resolution to accurately resolve turbulent structures is simply not computationally affordable. An approach which has proved to yield valuable results for turbulence prediction is the Large Eddy Simulation (LES) method, which separates the flow in large and small scale eddies to save computational effort [1].

Research has been done regarding the performance of various LES models for describing turbulent wind conditions in complex terrain. A comprehensive blind test including several models, called the Bolund experiment, has been conducted by Bechmann et al. [1], where the accuracy of these models across an isolated hill was tested. The performance of the LES models included in the analysis yielded somewhat disappointing results with significant speed-up errors over the Bolund Hill. One reason for the large deviations might be the challenge of obtaining the correct free stream boundary condition, which the LES models failed to do in this study [1]. A similar experiment has been done by Bechmann and Sørensen [2], where a hybrid RANS/LES model was tested over the Askervein Hill in Scotland. In this model, the near-wall regions are resolved in a Reynolds-Averaging manner with the two-equation k-Epsilon turbulence model. The model was able to predict

the high turbulence level in the complex wake region downwind of the hill reasonably well, but underestimated the mean velocity [2].

Experiments like Askervein Hill and Bolund Hill have provided invaluable insights into flow model performance and provided a benchmark for further flow model development. However, as wind power development expands into areas of even more complex terrain and challenging flow conditions, there is a need for full-scale validation cases which reflects the challenges the wind industry meets today. This paper presents a validation case in highly complex terrain, using a pulsed Doppler lidar. Lidars are particularly useful for this purpose as they can measure the spatial distribution of the wind along the lidar beam. However, there are limitations in the lidar technology that need to be addressed to obtain high-accuracy measurements.

Several studies have proven lidars to be reliable for measuring ten-minute mean velocities [3][4], but the research done regarding turbulence estimation shows that lidars are not able to accurately describe the turbulent features of the wind field. One of the main limitations of lidar systems is related to the spatial averaging along the lidar beam. This effect is most prominent in the accuracy of turbulence estimations when small fluctuations are of vital importance. Sjöholm et al. [5] investigated the spatial averaging effect for a ZephIR coherent wave lidar by comparing one-dimensional velocities with sonic measurements projected onto the line-of-sight (LOS) of the lidar. Two periods with different atmospheric conditions were investigated; one with low clouds and high backscattering, and one with clear conditions. The power density spectra were almost identical for low frequencies, but the lidar spectrum fell off more rapidly than the sonic spectrum for higher frequencies in both cases, proving that the lidar did not capture the small-scale turbulent features of the wind as accurately as the sonic anemometer. The spectra deviated at approximately 0.02 Hz in the clear conditions case and 0.05 Hz in the low cloud case with stronger backscattering. Cañadillas et al. [6] investigated the same effect for a WindCube pulsed lidar with a range gate length of $20\,\mathrm{m}$ on an offshore site. In this case, the power density spectra for line-of-sight velocities from the lidar and the sonic anemometer were only comparable up to a frequency of 0.21 Hz due to the scanning pattern of the lidar. The spectra showed a good compliance, and it was concluded that the spatial averaging along the lidar beam had a negligible effect for this range of frequencies.

Another important limitation of the lidar technology is that a horizontally homogeneous velocity field is assumed when deriving the three-dimensional wind field, which is not a valid assumption in complex terrain. Several studies regarding the performance of lidars in complex terrain have been conducted, among others by Guillén et al. [3] and Vogstad et al. [7]. Guillén et al. found that the deviation between ten-minute averaged lidar and cup anemometer measurements was significantly larger when the wind direction was such that the complex terrain features were most prominent. A greater discrepancy was also observed for higher turbulence intensities, and for higher vertical velocities [3]. Vogstad et al. [7] tested the performance of three different lidars; WindCube V1, ZephIR 300 and Galion/StreamLine in complex terrain by comparing measurements with cup anemometer data. A numerical flow model was used to correct for the inhomogeneities of the terrain when deriving the three-dimensional velocity field. They found that the uncertainty of the ten-minute averaged velocities from all lidars were in the order of 2.5% when applying the appropriate numerical corrections, which is comparable to the uncertainty of cup anemometers [7].

These studies [3][7] show that lidars may be used for point validations of the three-dimensional velocity field, but they are not capable of providing an estimate for turbulence validations without applying numerical corrections. The novel approach to flow model turbulence validation in this study uses a free-scanning lidar operating in fixed direction stare-mode aligned with the mean flow direction. This way, accurate estimations of the wind fluctuations along the line-of-sight may be derived, which can be used to validate how the flow model predicts the

variations of turbulence in the mean flow along the same line. The results can also give an indication of where the model succeeds or fails in predicting turbulence transport, production or dissipation.

In this study, the main objectives are to (1) evaluate the accuracy of 1D lidar measurements with a focus on turbulence estimation, (2) investigate a possible method to increase the accuracy of turbulence estimations with the lidar, and (3) use the lidar data to validate a computational flow model in highly complex terrain. Lidar line-of-sight measurements will be validated with sonic anemometer data projected onto the lidar beam, and the effect of spatial averaging will be investigated by changing the range gate length of the lidar. For the flow model validation, a hybrid RANS/LES (DES) model will be applied along a horizontal lidar beam parallel to the mean flow.

Fig. II.1: Map of the site with the position of the lidar (64°08'20.7"N 10°19'04.0"E) and the meteorological mast (64°08'09.7"N 10°19'00.7"E). The height contours represent $5\,\mathrm{m}$ height difference.

II. EXPERIMENTAL SETUP AND METHODOLOGY

The measurement campaign was carried out by Meventus in Roan in Sør-Trøndelag, Norway, with a ground-based StreamLine XR pulsed lidar in the proximity of a meteorological mast. In the following sections, a brief description of the site will be provided before the setup of the instruments and the methodology of the analysis will be explained.

A. Site Description

The site is located in central Norway, approximately $3\,\mathrm{km}$ from the coastline. The terrain at the site is complex, with rocky, mountainous and open topography. A steep ridge located $1300\,\mathrm{m}$ west of the lidar and mast is expected to generate complex flow with large-scale turbulent eddies. The positions of the lidar and mast, and the surrounding terrain are shown in Fig. II.1.

B. Experimental Setup for Lidar Validation

The triangular lattice mast is located at $366\,\mathrm{m}$ elevation. Cup anemometers are installed on the mast at different heights, and a 3D sonic anemometer is mounted at $98\,\mathrm{m}$ height. The StreamLine XR v14-8 lidar is located $344\,\mathrm{m}$
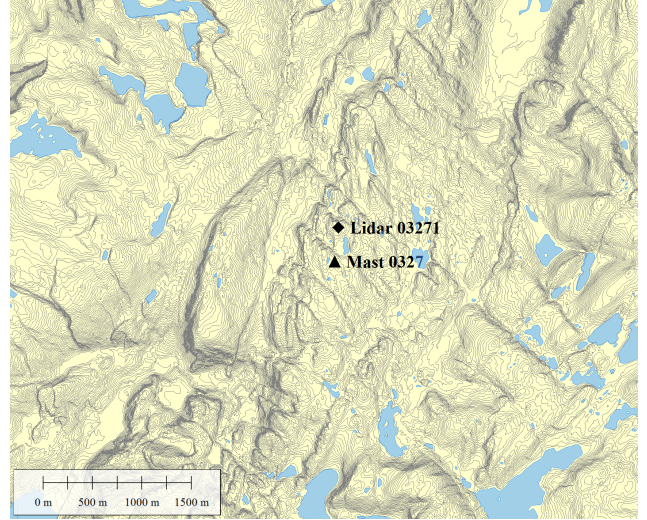
north of the mast at $370\,\mathrm{m}$ elevation. The range gate length of the lidar is $18\,\mathrm{m}$.

The lidar was programmed to perform different scanning operations depending on the observed wind conditions. With southerly and northerly winds, the lidar was operating in stare-mode, i.e. with constant azimuth and elevation angles, towards the sonic anemometer. Due to an error in the measurement campaign design, the lidar was operating with an error in azimuth angle of $0.08°$, causing it to measure $\sim 0.5\,\mathrm{m}$ to the right of the sonic anemometer. This is not expected to have a significant impact on the results.

Line-of-sight velocities from the lidar were collected with a sampling frequency of 1 Hz throughout a two-month period from 13.04.2015 to 11.06.2015. Corresponding horizontal and vertical velocities and wind directions were collected with the sonic anemometer for the same period. A mounting error in the direction of the sonic anemometer of $-7°$ was detected and corrected for. This was done by observing how the correlation between the lidar and sonic anemometer data changed when adding an error term to the direction measured by the sonic anemometer. The correlation was highest when subtracting $7°$, indicating that this is the true

wind direction. Fig. II.2 illustrates the setup of the two instruments.
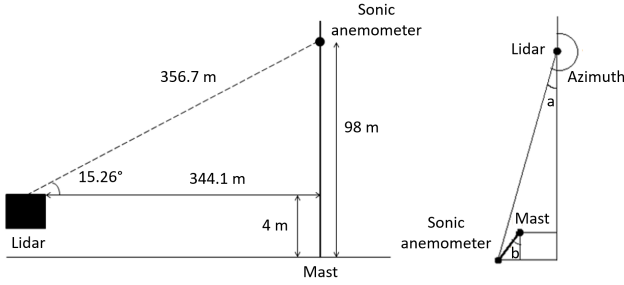

Fig. II.2: Schematic of the lidar and mast positions. *Left:* side view of the setup. The elevation angle is 15.26°. *Right:* top view of the setup. Azimuth angle = 180° + a, a = 6.86°. The azimuth angle used in the campaign is 186.94°, causing a deviation of ∼0.5 m (0.08°) from the sonic anemometer. The sonic anemometer is mounted on a 5 m long boom at an angle b = 45°.

1) Data Analysis:

The sonic anemometer measurements were projected onto the line-of-sight of the lidar to allow for a comparison of one-dimensional velocities along the lidar beam. The sonic anemometer measurements were related to grid north by correcting for a difference of 1.18° between geographical and grid north at the site. The lidar measurements were corrected for a bearing of 1.1° from grid north, calculated from GPS measurements.

To provide information about the quality of the lidar data, these include values for the pitch and roll angles and the intensity of the backscattered signal. The pitch and roll angles are the forward/backward and sideways tilt angles of the lidar. During the measurement period, these were checked remotely to be within a 0.25° threshold. This yields a maximum deviation of 1.55 m of the beam from the sonic anemometer. When validating the lidar data, a stronger filtration of these values was performed to ensure that the beam deviation was within 1 m, corresponding to a maximum 0.16° pitch and roll angle. The intensity, defined by equation II.1, is a measure of the strength of the backscattered signal.

$$Intensity = 1 + SNR \qquad \text{(II.1)}$$

SNR is the signal-to-noise ratio of the signal. An analysis was carried out to determine how the correlation of the lidar and sonic anemometer data was affected by filtration of intensity values.

Velocity measurements and turbulence intensity estimates were compared using standard linear regression analysis. The turbulence intensity along the line-of-sight (LOS) is given by equation II.2 [8].

$$TI_{los} = \frac{\sigma_{los}}{\overline{U_{los}}} \qquad \text{(II.2)}$$

The coefficient of determination R^2, defined by equation II.3 [9] for data sets x and y, was used as a measure of the correlation between the lidar and sonic anemometer measurements.

$$R^2 = \frac{(\sum(x - \overline{x})(y - \overline{y}))^2}{\sum(x - \overline{x})^2 \sum(y - \overline{y})^2} \qquad \text{(II.3)}$$

A spectral analysis was performed for a more detailed comparison of the data. Power density spectra illustrate how the energy is transferred from larger to smaller eddies. As a reference, the spectra were compared with the theoretical Kolmogorov slope of -5/3 in the inertial subrange [10].

The effect of changing the range gate length of the lidar was investigated by reprocessing raw lidar data in the program Raw Data Processor v14 developed by Halo Photonics. A 24 hour period on 30.04.2015 with large variations in wind velocity and direction was chosen for this analysis to challenge the lidar with varying wind conditions. The wind velocity and direction measured by the sonic anemometer during this period are illustrated in Fig. II.3. Data were reprocessed with range gate lengths of 9 m and 30 m.

C. Experimental Setup for DES Model Validation

The large-scale turbulent structures of interest in this study are expected to be generated downwind of the ridge located approximately 1300 m southwest of the lidar. The ridge has a steep vertical cliff with an elevation of 150 m facing westward. For the purpose of validating
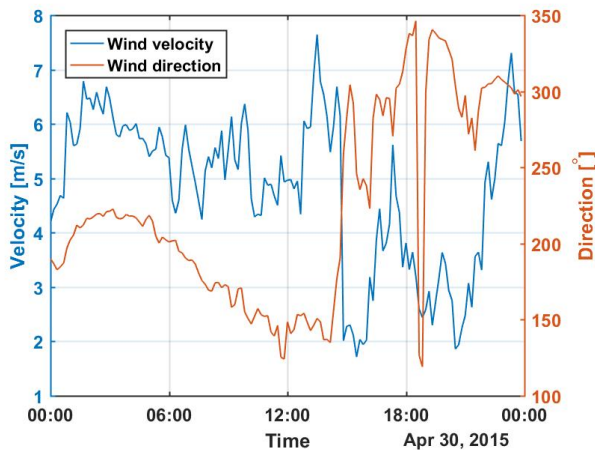
Fig. II.3: Wind velocity and direction during 30.04.2015 measured by the sonic anemometer.

the flow model, the lidar was operating in stare-mode towards this ridge, parallel to the mean flow as shown in Fig. II.4. The velocity was measured along the length of the beam, and the locations a)-c) were used for a more detailed spectral analysis.
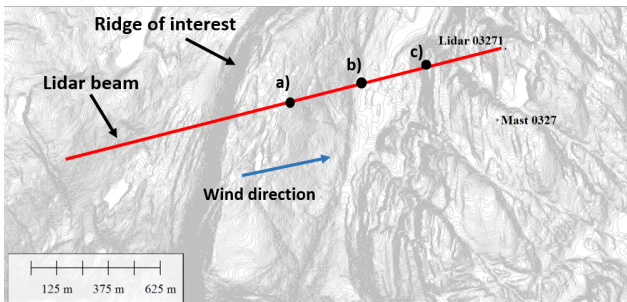

Fig. II.4: Map describing the location of the lidar and meteorological mast, and the ridge of interest to the study. Flow model results were compared with lidar measurements along the line-of-sight parallel to the mean flow, and points at distances a) $1000\,\mathrm{m}$, b) $600\,\mathrm{m}$ and c) $400\,\mathrm{m}$ from the lidar were used for further evaluations.

A detailed assessment of wind data from a cup anemometer at $100\,\mathrm{m}$ height at the mast was used to identify a period with steady wind speeds and wind direction approximately orthogonal to the ridge. The estimated Monin-Obukhov length scale [11] was found to be near-neutral ($|MOL| > 450$) for the entire period, implying that the vertical heat flux is close to zero. The conditions during the selected time period are presented in Table II.1.

Initially, a systematic bearing for the lidar of $1.7°$ from grid north was detected by binocular measurements. To account for this bearing, the lidar was operating with an azimuth angle of $262°$ to align with the mean wind direction ($260°$). At a later stage in the measurement campaign, GPS calculations were performed suggesting the offset to be $1.1°$. Hence, there was an error between $0.3°$ and $0.9°$ between the lidar beam and the mean wind direction. An elevation angle of $2°$ was used to prevent the lidar beam to intersect with the ground.

1) Simulation Procedure:

Classical methodology regarding wind farm modeling using computational fluid dynamics (CFD) refers to two general strategies: the Reynolds Averaged Navier-Stokes (RANS) and Large Eddy Simulation (LES) methods. In the RANS method, the simulation is executed aiming for a steady state solution, for which the turbulent properties are modeled in the framework of applied transport models. As a result, the transient behavior of turbulent flows is suppressed. The general principle of the LES method is to resolve the turbulent structures in the main flow, i.e. the large eddies, and model the effect of the smaller eddies. Although this approach will yield more realistic results, the computational cost is much higher [12].

Due to the filtering of large and small eddies, LES models encounter severe difficulties in the near-wall region, for which the correct physical characteristics cannot be reproduced due to insufficient mesh resolution. This is a significant problem for atmospheric boundary layer flows with high Reynolds numbers, as the mesh requirement becomes computationally unaffordable. To solve this issue, a Detached Eddy Simulation (DES) is used in this study. A DES is a hybrid RANS/LES method which compensates this shortcoming by applying the RANS model in the near-wall region. The switch from LES to RANS is based on the to-wall distance, as well as the modeling length scale and cell size [2]. The hybrid RANS/LES approach selected for this numerical study was first proposed by

8

TABLE II.1: Wind conditions observed during the selected time period.

Time period	Wind speed @100 m Mean (min, max) [m/s]	Wind direction @100 m Mean (min, max) [°]	Monin-Obhukov length scale (min) [m]
14.06.2015 13:00-22:30	8.3 (7, 10)	260 (250, 290)	(450)

Spalart [12]. Details about the transport models, as well as the filtering strategies are described by Bechmann et al. [2].

The computational domain was constructed by Fraunhofer IWES' terrainMesher, and the simulations were performed by Fraunhofer IWES in OpenFOAM. A region covering a $9.5\,\text{km}$ x $7.3\,\text{km}$ area orthogonal to the wind direction was meshed by ∼56 million degrees of freedom, with increasing mesh resolution near the surface. The governing equation system is the Navier-Stokes equations, and the RANS and LES flow models are applied without heat transfer (neutral conditions).

The inlet condition with a mean bulk velocity of 8.3 m/s was first estimated by a RANS simulation using the k-Epsilon turbulence model. This simulation also served as the starting point for the DES simulation. However, to obtain the required eddy structures in the inlet profile for the DES simulation, a prolonged inlet with circulating flow was used. The velocity fluctuations were triggered by surface shear which caused an instability in the momentum equation. The domain with the prolonged inlet is shown in Fig. II.5.
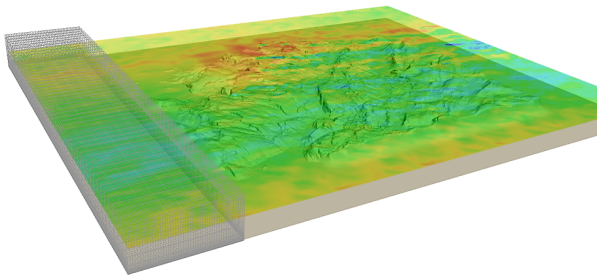

Fig. II.5: Illustration of the computational domain with the prolonged inlet. The ridge of interest can be seen in the center of the domain.

The DES simulation was executed over 25000 physical seconds, which corresponds to approximately 20 flow through times (FFT). The results were averaged over 15 FFT, which can demon-strate a plausible statistical representation. The simulation results were extracted along a line parallel to the mean flow, i.e. at an azimuth angle of $260°$. Due to a misrepresentation of the terrain, the simulation results intersected the surface at an elevation angle of $2°$. To solve this issue, the results were extracted using an elevation angle of $3°$.

A spectral analysis was performed for a few locations along the beam. The spectra were compared with the predicted Kaimal spectrum for the longitudinal wind speed, which is given by equation II.4 [13].

$$\frac{nS_u(n)}{u_*^2} = \frac{105f}{(1 + 33f)^{5/3}} \quad \text{(II.4)}$$

u_* is the friction velocity, S_u is the power density for the longitudinal wind and f is the normalized frequency, related to frequency n, height z and velocity U(z) by relation II.5.

$$f = \frac{nz}{U(z)} \quad \text{(II.5)}$$

The friction velocity is estimated using the logarithmic law, given by equation II.6 [14].

$$u(z) = \frac{u_*}{K} ln\left(\frac{z}{z_0}\right) \quad \text{(II.6)}$$

K is the von Karman constant (= 0.4) [14], and z_0 is the surface roughness which is approximately $0.03\,\text{m}$ for bare mountains [15]. The friction velocity is estimated at $100\,\text{m}$ height at the measurement mast. Using the mean velocity of 8.3 m/s yields a friction velocity of 0.41 m/s.

III. RESULTS AND DISCUSSION

In this section, a validation of the lidar will be presented by comparison with sonic anemometer data. Next, the effect of changing the range gate length of the lidar will be analyzed. Lastly, lidar measurements will be used to validate a numerical DES flow model.

A. Validation of Lidar Measurements

For evaluating the accuracy of turbulence estimates with the lidar, the data were compared to sonic anemometer measurements with a sampling frequency of 1 Hz. As an initial analysis, the effect of the level of filtration of lidar data was investigated. Noisy measurements were removed by increasing the filtering limit on the intensity value of the lidar signals, and the correlation between the lidar and sonic anemometer data were evaluated for increasing values. Fig. III.1 shows how the coefficient of determination changes with the limiting intensity value, and how the availability of measurements is affected.

Fig. III.1: Coefficient of determination R^2 and availability versus the lower intensity limit. The total number of measurements during the time period is 5.1×10^6, and the number of measurements towards the sonic anemometer is 2.55×10^6.

The figure shows that the coefficient of determination has a maximum value of $R^2 = 0.9454$ with an optimal intensity limit of 1.1. The slope of the linear regression line for this limit is 0.9705. With a higher limit, the reduction of availability will dominate and cause a decrease in the coefficient of determination. This effect occurs because the differences between the lidar and sonic anemometer measurements are amplified for large and rapid (fluctuating) changes in velocity, which typically occurs across long time gaps.

Note that the availability of measurements is low (less than 50%) for all limiting values of the intensity in Fig. III.1. This is mostly because

there are missing periods in the data set when the lidar has been occupied performing other scan patterns, and not scanning towards the sonic anemometer. When increasing the intensity limit, periods with clear conditions are also filtered out. Fig. III.2 illustrates how the temperature, relative humidity, and intensity are related. In clear conditions with low humidity and high temperature, the intensity is low due to a lack of particles in the air and hence a weak backscattering. It can be seen that the intensity is close to the lowest limit used in the analysis in Fig. III.1 (1.01) during clear-condition periods. With the optimal intensity limit of 1.1, the availability is reduced to 37% due to a loss such periods. The figure only shows a time period of 24 hours on 30.04.2015, but the illustrated phenomenon is applicable for all times and causes a loss of clear-condition periods with higher intensity limits.
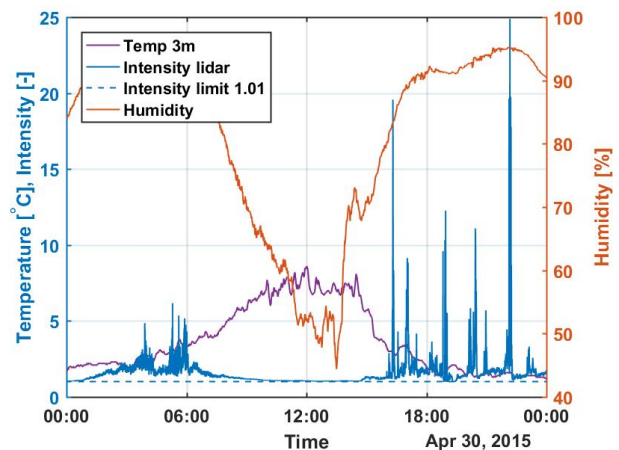

Fig. III.2: Temperature, relative humidity and intensity versus time for a 24 hour period on 30.04.2015. The lowest intensity limit used in the analysis of 1.01 is included as a reference.

In Fig. III.3, the one-dimensional wind velocity measured with the lidar and the sonic anemometer with a sampling frequency of 1 Hz and the optimal intensity limit of 1.1 are plotted as a function of time. The lidar measurements follow the sonic measurements very well, although the sonic anemometer captures more fluctuations than the lidar. As explained in section I, the spatial averaging along the lidar beam removes some of the small-scale features
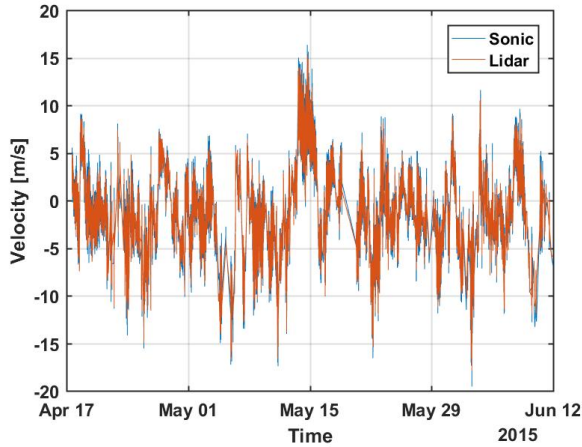
Fig. III.3: Time series of one-dimensional 1 Hz velocities from 13.04.2015 - 11.06.2015 measured with the lidar and the sonic anemometer.
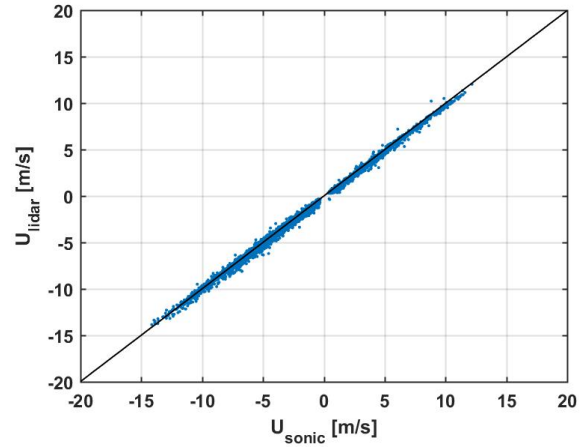

Fig. III.4: Correlation plot of ten-minute averaged velocities from 13.04.2015 - 11.06.2015. The coefficient of determination is $R^2 = 0.9972$ and the linear regression slope is 1.0043.

of the wind, and hence the small fluctuations are not described as accurately as with the sonic anemometer. Similar results were observed by Sjöholm et al. [5].

Fig. III.4 shows a correlation plot of one-dimensional ten-minute averaged velocities from the lidar and the sonic anemometer. The coefficient of determination during this period is $R^2 = 0.9972$, and the linear regression slope is 1.0043. The figure confirms the lidars' ability to obtain accurate mean velocities. The ten-minute averaged velocities correlate almost perfectly and are comparable with results from similar experiments done in previous research [4][7].

Fig. III.5 shows a correlation plot with the optimal intensity limit of 1.1 and a sampling frequency of 1 Hz. There is a larger spread in this case than for the ten-minute averaged velocities in Fig. III.4, which is also reflected in the lower coefficient of determination $R^2 = 0.9454$ and slope of the linear regression line 0.9705.

In Fig. III.6, the turbulence intensities along the line-of-sight estimated by the lidar and the sonic anemometer are plotted as a function of velocity. There is a larger spread for low velocities, and the deviations decrease with increasing velocity. Considering equation II.2, it is clear that the value of the turbulence intensity is more sensitive to small changes in $\overline{U}$ for low velocities, causing a larger spread. On a mean level,
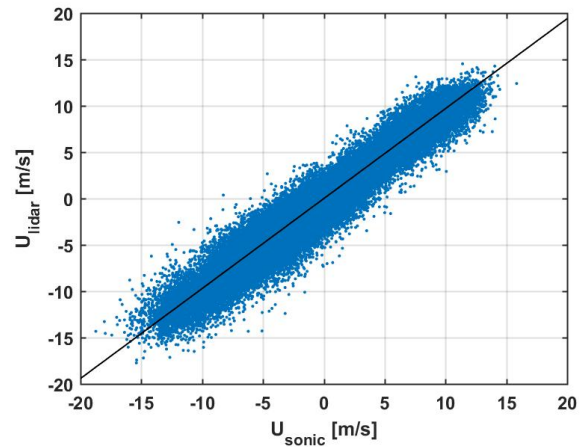

Fig. III.5: Correlation plot of one-second velocities from 13.04.2015 - 11.06.2015. The coefficient of determination is $R^2 = 0.9454$ and the linear regression slope is 0.9705.

the lidar slightly underestimates the turbulence intensity.

Fig. III.7 shows the power density spectra for the lidar and the sonic anemometer as well as the theoretical Kolmogorov -5/3 slope for the inertial subrange [10].

Both spectra have a steeper slope than the theoretical Kolmogorov slope. This is most likely due to the low availability of 37% with the optimal intensity limit. With low availability, there are several time gaps in the data set which are ignored when computing the power density spectra. The changes over these time gaps will
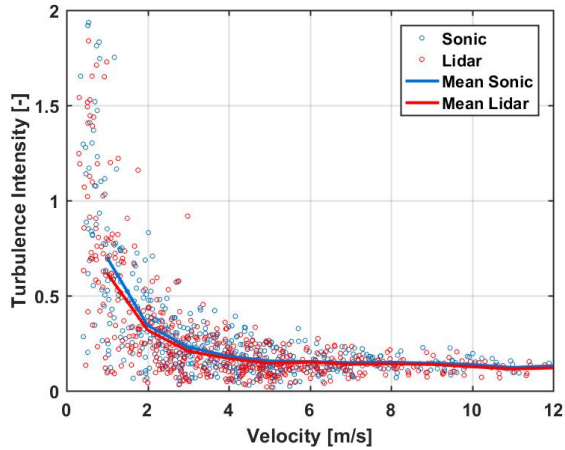
11

Fig. III.6: Turbulence intensity versus velocity for the lidar and the sonic anemometer.
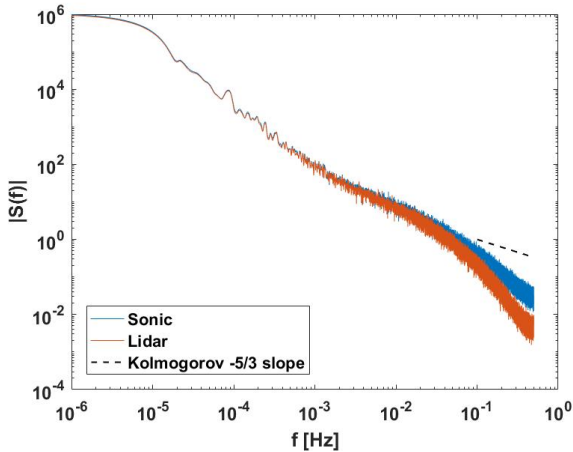

Fig. III.7: Power density spectra for the lidar and the sonic anemometer, and the theoretical Kolmogorov slope.

be detected as a change over one second and will contribute to an erroneous power density level.

The figure also shows that the lidar spectrum has a lower power density for higher frequencies than the sonic anemometer spectrum. Hence, the lidar does not capture the small-scale turbulent features of the wind as accurately as the sonic anemometer due to the spatial averaging along the lidar beam. The deviation between the spectra occurs at approximately 0.03-0.07 Hz. Similar results were observed by Sjöholm et al., with a deviation in the spectra at 0.02-0.05 Hz [5]. As mentioned in section I, Cañadillas et al. concluded that the spatial averaging had a negligible effect up to 0.21 Hz [6]. In their

analysis the availability was over 90%, which might be a reason for the favorable results.

B. Effect of Range Gate Length

Fig. III.8 shows how the coefficient of determination changes with the intensity limit for the different range gate lengths during the 24 hour analysis period on 30.04.2015. It can be seen that R^2 is higher for longer range gate lengths with low intensity limits (< 1.1), and higher for shorter range gate lengths with higher limits (> 1.1). This is because the intensity of the signal decreases when the range gate length is shortened. With a short range gate length, the amount of noisy measurements with low intensity is larger, contributing to a lower correlation. However, when the noisy measurements are removed as the intensity limit is increased, a shorter range gate length with a smaller spatial averaging effect gives a better correlation than a longer range gate length.
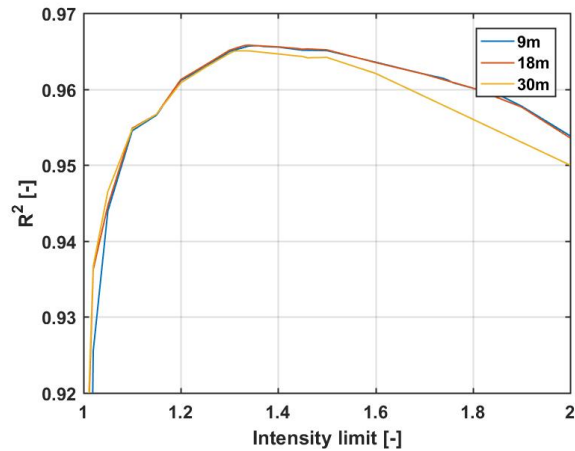

Fig. III.8: Coefficient of determination versus lower intensity limit for the three different range gate lengths on 30.04.2015.

Table III.1 summarizes the optimal case for each range gate length. The table shows that the optimal intensity limit is higher for shorter range gate lengths. This appears to be because the smaller spatial averaging effect with shorter range gate lengths dominates the effect of reduced availability. Thus, the intensity limit can be increased further before the correlation decreases, notwithstanding the reduced availability.

12

TABLE III.1: Optimal R^2 values and the corresponding intensity limit and availability for the different range gate lengths. The total number of measurements during the time period is 85729, and the number of measurements towards the sonic anemometer is 74462.

Range gate length [m]	Opt. R^2 [-]	Opt. intensity limit [-]	Availability [%]
9	0.9657	1.36	48.1
18	0.9657	1.34	49.7
30	0.9650	1.32	50.4

Note that the optimal intensity limit is higher with the original $18\,\mathrm{m}$ range gate length for this period (1.34) than for the longer period discussed in section III-A (1.1). For the longer two-month period, the availability was very low also for low intensity limits, causing the decrease in R^2 to happen at a lower intensity value than for this period.

In Fig. III.9, the power density spectrum for the sonic anemometer is plotted together with the lidar spectra using different range gate lengths. The data were filtered with an intensity limit of 1.32 to obtain the best possible correlation for all range gate lengths, before concurrent measurements were plotted.
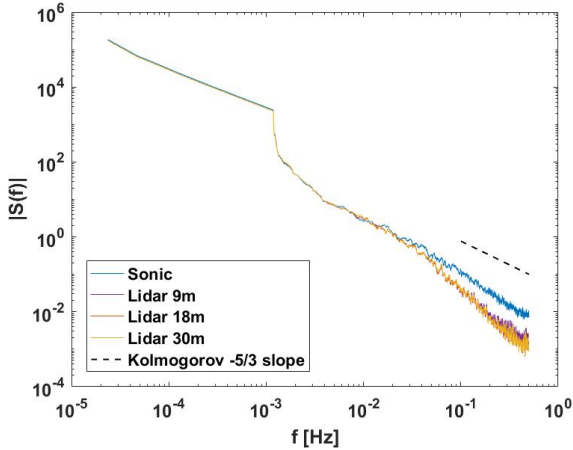

Fig. III.9: Power density spectra for the lidar with different range gate lengths, the sonic anemometer and the theoretical Kolmogorov slope.

The sonic spectrum is almost parallel with the Kolmogorov slope in the inertial subrange. The availability for this period is approximately 50%, which might explain the gentler slope and more accurate power density level compared to the spectra in Fig. III.7. The lidar spectra have a steeper slope than the sonic spectrum, and the deviation occurs at approximately 0.05 Hz for all three range gate lengths. However, a higher power density is obtained with a range gate length of $9\,\mathrm{m}$ for the very highest frequencies. This proves that slightly more turbulence information is captured using the shortest range gate length tested in this study. The spectra for $18\,\mathrm{m}$ and $30\,\mathrm{m}$ range gate lengths look very similar, suggesting that the improvement is smaller by reducing the range gate length from $30\,\mathrm{m}$ to $18\,\mathrm{m}$ than from $18\,\mathrm{m}$ to $9\,\mathrm{m}$ with a fixed intensity limit.

The sharp drop in power density at approximately 10^{-3} Hz is most likely related to the scanning pattern of the lidar. The staring periods towards the sonic anemometer comprise 600 measurements, interrupted by changes in azimuth and elevation. This results in a rapid change of power density at $1/600 \approx 1.67 \mathrm{x} 10^{-3}$ Hz.

C. Validation of DES Model

In Fig. III.10, the velocity computed with the DES model averaged for 15 FFT and the lidar measurements averaged for the time period 14.06.2015 13:00-22:30 are plotted along the lidar beam parallel to the mean flow. The velocity is normalized by the upstream free flow velocity at $250\,\mathrm{m}$ from the lidar, which is a suitable location to place a meteorological mast. The DES model underestimates the speed-up over the ridge at approximately $1300\,\mathrm{m}$ from the lidar and overestimates the wind deficit downwind the ridge. Here, the DES results are obtained in the wall-function region, where the RANS model is applied. Closer to the lidar, the DES model provides good estimates for the wind speed variations along the line-of-sight.

Similar results were observed by Bechmann et al. for the Askervein Hill. For the complex flow region downwind of the hill, the DES model was found to overestimate the flow separation and hence underestimate the velocity [2]. The velocity underestimation in this study might be due to a similar flow separation downwind of the ridge at $1300\,\mathrm{m}$.
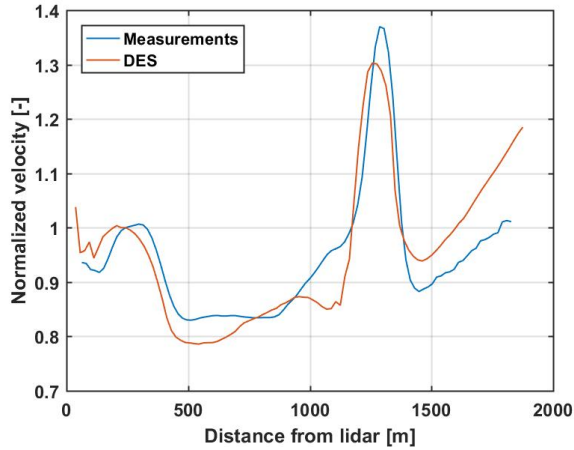
Fig. III.10: Velocity along the lidar beam normalized by the upstream free flow velocity averaged for 14.06.2015 13:00-22:30 measured by the lidar and computed with the DES model.
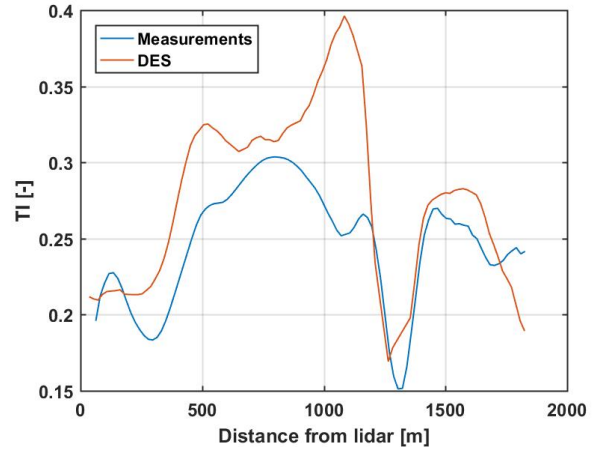

Fig. III.11: Turbulence intensity along the lidar beam averaged for 14.06.2015 13:00-22:30 estimated by the lidar and computed with the DES model.
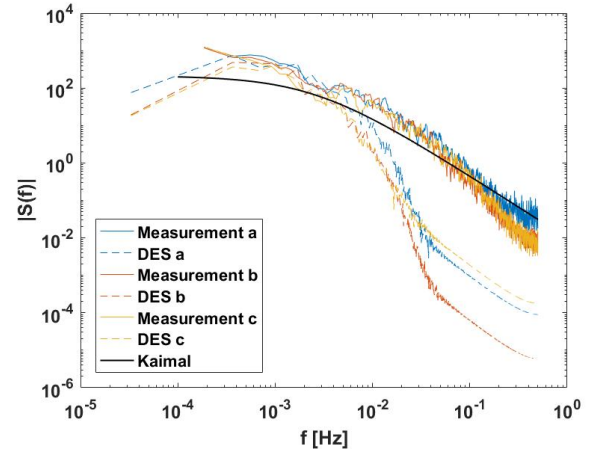
Fig. III.11 shows the turbulence intensity along the lidar beam estimated by the lidar and computed with the DES model averaged for the same time period. The DES model overestimates the turbulence intensity for most of the lidar beam. However, the variations along the beam are captured. The overestimate seems to be connected to the wind speed deficit downwind of the ridge.

Bechmann et al. concluded that the DES model was able to predict the turbulence level on the lee side of the Askervein Hill [2]. However, the Askervein Hill is only moderately complex and the surrounding terrain is flat. The overestimation in this study might be due to the complexity of the terrain causing a highly complex wind flow and a higher computational uncertainty.

A spectral analysis was performed at three different distances from the lidar (a) $1000\,\mathrm{m}$, b) $600\,\mathrm{m}$ and c) $400\,\mathrm{m}$), and the results were compared to the predicted Kaimal spectrum for the longitudinal wind based on the measured wind speed at $100\,\mathrm{m}$ at the measurement mast. The power density spectra for the lidar and the DES model at the three locations are plotted in Fig. III.12 together with the predicted Kaimal spectrum.

The figure shows how the model manages to predict the low-frequency part of the spectra for

Fig. III.12: Power density spectra for the lidar and the DES model at distances a) $1000\,\mathrm{m}$, b) $600\,\mathrm{m}$ and c) $400\,\mathrm{m}$ from the lidar, and the estimated Kaimal spectrum during 14.06.2015 13:00-22:30.

all locations. For the very lowest frequencies ($< 2\mathrm{x}10^{-4}$), the lidar spectra are undefined due to gaps in the time series. There is a significant cut-off in the higher frequencies at $\sim 4\mathrm{x}10^{-3}$ Hz due to uncertainty related to the complexity of the terrain and insufficient mesh resolution to capture the small-scale fluctuations.

For the lidar measurements, the spectrum for location a) has a higher power density than for location b) and c) for the highest frequencies, suggesting that the turbulence level is higher at location a). Considering the ridge at $1300\,\mathrm{m}$ from the lidar, this is an expected result. For

the DES model on the other hand, a higher power density is obtained for location c) than locations a) and b) for the highest frequencies. As location c) is closer to the ground where the mesh resolution is finer, the model might be able to capture the turbulent eddies to a greater degree at this location. However, due to the uncertainties related to the computational model in the high-frequency region, the results here are not fully reliable.

The predicted Kaimal spectrum underestimates the power density for most frequencies ($< 10^{-1}$ Hz). The model is based on shear-introduced turbulence [13], and these results suggest that the model is not able to capture the additional mechanically induced turbulence due to the complexity of the terrain. For higher frequencies, the model is a good fit for location a) with a higher turbulence level. Nontheless, as the model is based on the measured speed at $100 \, \text{m}$ height, the model is not expected to be a highly accurate fit.

Note that there is a difference in the azimuth angle between $0.3°$ and $0.9°$ and elevation angle of $1°$ between the measured and modeled results. The resulting deviations in the horizontal and vertical directions at the three locations along the beam are presented in Table III.2

TABLE III.2: Horizontal and vertical deviations at the three locations along the beam caused by the difference in azimuth and elevation angle between the measured and modeled results.

Location	Horizontal deviation (min, max) [m]	Vertical deviation [m]
a)	(5.24, 15.71)	17.45
b)	(3.14, 9.42)	10.47
c)	(2.09, 6.28)	6.98

Even though the error introduced is non-negligible, it can be disregarded considering the resolution of the mesh and the uncertainties involved in predicting the wind regime in this terrain.

IV. CONCLUSIONS

In this study, the performance of a hybrid RANS/LES (DES) flow model for turbulence estimation has been evaluated by comparison with lidar measurements in highly complex terrain.

First, the accuracy of turbulence estimates with the lidar was evaluated by validation with sonic anemometer data. The analysis proved the lidar to be very accurate in prediction of mean velocities, but a lower correlation was observed for a sampling frequency of 1 Hz. As expected, small fluctuations are not captured due to the spatial averaging along the lidar beam. The possibility of increasing the accuracy of the lidar was investigated by changing the range gate length. With a shorter range gate length, the spatial averaging effect is smaller, but the relative noise level is increased. A slight improvement was observed by reducing the range gate length to $9 \, \text{m}$ with sufficient filtration of noisy data, but the resulting reduction of data availability is a disadvantage. As the uncertainties related to the spatial averaging of the lidar are relatively small compared to uncertainties in the computational model, the accuracy of the lidar for validation of flow model turbulence estimations might be considered sufficient with all three range gate lengths used.

The performance of the DES model for turbulence estimation was tested by comparison with lidar measurements along a beam aligned with the mean flow, pointing towards a steep ridge. The model was able to describe the variation of velocity and turbulence along the beam. However, the model overestimated the mean turbulence level, and failed to accurately describe the acceleration upwind and deceleration downwind of the ridge. The deviations are assumed to be related to the mesh resolution and uncertainties in the computational model for the high complexity of the terrain.

For further work, the DES results may be extracted along the actual line-of-sight of the lidar to eliminate the error induced from difference in azimuth and elevation angles. Note that the results may only be compared up to the point where the DES model intersects with the surface. Additionally, the applicability of the DES model in different flow regimes and situations will be useful to investigate.

REFERENCES

[1] Bechmann, A., Sørensen, N. N., Berg, J., Mann, J., and Réthoré, P. E. The Bolund Experiment, Part II: Blind Comparison of Microscale Flow Models. *Boundary-Layer Meteorology*, 141(2):245–271, 2011.

[2] Bechmann, A. and Sørensen, N. N. Hybrid RANS/LES Method for Wind Flow Over Complex Terrain. *Wind Energy*, 13(1):36–50, 2010.

[3] Guillén, B. F., Gómez, P, Rodrigo, S. J., Courtney, M. S., and Cuerva, A. Investigation of Sources for Lidar Uncertainty in Flat and Complex Terrain. *Proceedings of EWEC-11, Brussels, Belgium*, 2009.

[4] Sathe, A., Mann, J., Gottschall, J., and Courtney, M. Can Wind Lidars Measure Turbulence? *Journal of Atmospheric and Oceanic Technology*, 28(7):853–868, 2011.

[5] Sjöholm, M., Mikkelsen, T., Mann, J., Enevoldsen, K., and Courtney, M. Spatial Averaging-Effects on Turbulence Measured by a Continuous-Wave Coherent Lidar. *Meteorologische Zeitschrift*, 18(3):281–287, 2009.

[6] Cañadillas, B., Westerhellweg, A, and Neumann, T. Testing the Performance of a Ground-Based Wind LiDAR System: One Year Intercomparison at the Offshore Platform FINO1. *Dewi Magazin*, 38(5), 2011.

[7] Vogstad, K., Simonsen, A. H., Brennan, K. J., and Lund, J. A. Uncertainty of Lidars in Complex Terrain. In *EWEA 2013*, 2013.

[8] Kumer, V.-M., Reuder, J., Dorninger, M., Zauner, R., and Grubišić, V. Turbulent Kinetic Energy Estimates From Profiling Wind LiDAR Measurements and Their Potential for Wind Energy Applications. *Renewable Energy*, 99:898–910, 2016.

[9] Walpole, R. E., Ye, K., Myers, S. L., and Myers, R. H. *Probability and Statistics for Engineers and Scientists*. Pearson Education International, 8th edition, 2007.

[10] Pope, S. B. *Turbulent Flows*. Cornell University, 2000, pages 182–191.

[11] Monin, A. S. and Obukhov, A. M. Basic Laws of Turbulent Mixing in the Surface Layer of the Atmosphere. *Tr. Akad. Nauk SSSR Geophiz. Inst*, 24(151):163–187, 1954.

[12] Spalart, P. R. Strategies for Turbulence Modelling and Simulations. *International Journal of Heat and Fluid Flow*, 21(3):252–263, 2000.

[13] Kaimal, J., Wyngaard, J., Izumi, Y, and Coté, O. Spectral Characteristics of Surface-Layer Turbulence. *Quarterly Journal of the Royal Meteorological Society*, 98(417):563–589, 1972.

[14] Beaupuits, J. P. P., Otárola, A, Rantakyrö, F., Rivera, R., Radford, S., and Nyman, L. Analysis of Wind Data Gathered at Chajnantor. *ALMA Memo*, 497, 2004.

[15] Weir, D. E. Vindkraft - Produksjon i 2013. *Norges Vassdrags- og Energidirektorat*, 2014.